Model of ultrashort-pulse laser excitation of bulk and thin film dielectrics: Coupling material excitation and electric field propagation

Peter S. Sneftrup⊙, Søren H. Møller⊙, and Peter Balling⊙
Department of Physics and Astronomy, Aarhus University, Ny Munkegade 120, 8000 Aarhus C, Denmark

The interaction of ultrashort laser pulses with dielectrics is associated with strong coupling between the material response and the light. The ultrashort pulses excite the materials, and the corresponding rapid changes in optical properties, induced by the generation of free carriers, determine the propagation of the light. In this paper, we describe a self-consistent model for this interaction. The material excitation is described by a model in which the electron dynamics is captured by a set of multiple rate equations coupling energy levels in a conduction band that has been discretized into energy states separated by the photon energy. The propagation of the light is calculated from Maxwell's equations using the finite-difference time-domain approach. The model is used to calculate key observables from laser ablation experiments, e.g., the threshold fluence versus pulse duration and the depth of laser-ablated structures versus fluence, for bulk and thin film samples. For both freestanding thin samples and dielectric stacks, corresponding to high-reflectivity mirrors, the results of the model are strongly influenced by interference phenomena, which significantly influence the material response and ablation. The model is compared to an existing approach using propagation of the intensity envelope of the pulse. In the absence of interference, the two methods predict almost identical ablation thresholds as well as hole depths.

I. INTRODUCTION

When wide-band-gap dielectrics are exposed to ultrashort laser pulses, the high intensities cause a large number of valence-band electrons to be excited to the conduction band [1,2]. For sufficiently high excitation levels, the material may become unstable, and material will be ejected from the surface. This is referred to as laser ablation. Laser ablation of dielectrics has been studied extensively for the past three decades [3–7], and the literature agrees that for pico- and femtosecond pulses, three different processes are necessary to describe the material response that eventually causes laser ablation in dielectrics: (1) strong-field excitation of valence-band electrons [8,9], (2) plasma absorption of excited carriers [1,2], and (3) collisional excitation by which energetic conduction-band electrons can promote valence-band electrons to the conduction band [1,2]. For sufficiently long pulses, the latter process can lead to carrier multiplication in a so-called avalanche process [3].

These physical processes have, for the last two decades, been incorporated into various numerical models for describing short-pulse laser ablation of dielectrics and predict physical observables in ablation experiments. The first of these models was the *single rate equation* (SRE) model [3,10,11], in which the conduction band is considered a single energy level. Although the SRE model has demonstrated qualitative agreement with experimental data of ablation thresholds [11–13], it lacks the ability to properly incorporate the electron heating needed to induce collisional excitation [14] and hence breaks down for long pulse durations, where avalanche excitation is relevant [15–17]. A more sophisticated model was proposed by Kaiser *et al.* [18] based on the

Boltzmann equation, which included all relevant mechanisms and was used to predict the ablation threshold and its dependence on pulse duration. Based on this model's prediction of the energy distribution of conduction-band electrons immediately after excitation, an improved rate-equation model was proposed by Rethfeld [14] in which the conduction band was discretized into multiple energetically equidistant levels. This model was called the *multiple rate equations* (MRE) model and has since been improved to also include propagation [5] and has shown agreement with experimental data [2,19,20].

In previous implementations of the MRE model, the propagation of the laser pulse was described in terms of intensity [5], using a Drude model for the optical response to calculate the plasma absorption and thereby propagating the pulse in terms of its intensity envelope [21]. In this paper, we propose a model of laser excitation of dielectrics in which the laser pulse is propagated in terms of the electric field while the material excitation is described by the MRE model. Several other studies have used similar approaches of simultaneously solving Maxwell's equations with the inclusion of material excitation [22–26], some using three-dimensional field propagation [23–26], including carrier diffusion [26], and investigating the effects of interference in coatings [24]. Rather than relying on variations of the SRE model [22–26] to describe the material excitation, in the present paper we use the more complete description given by the MRE model. We compare the present model to results based on intensity propagation and discuss their similarities and differences. Additionally, we perform calculations on thin films and coatings and confirm that the model corroborates the expectation of excitation being predominantly localized near regions of constructive interference [27]. We demonstrate, in the case of a single freestanding thin

film, how the fluence of the laser pulse directly determines how many constructive interference layers are ejected from the material, as reported experimentally by Kumar *et al.* [28] and Roper *et al.* [29].

II. NUMERICAL MODEL

A. Optical response of laser-excited dielectrics

The MRE model used in this paper calculates the density of electrons excited to the conduction band. How these conduction-band electrons affect the propagation of a laser pulse through the excited dielectric depends on the optical model. Here, we make use of the Drude model to describe the dielectric function, which is related to the *complex* refractive index $\tilde{n}(\omega) = n(\omega) + i\kappa(\omega) = \sqrt{\epsilon(\omega)}$ [1,2],

$$\epsilon(\omega) = \epsilon_B - \frac{\omega_p^2}{\omega^2 + i\omega\Gamma}, \tag{1}$$

where ϵ_B is the background permittivity, ω_p is the plasma frequency, ω is the central angular frequency of the laser pulse, and Γ is the scattering rate. The background permittivity ensures that the material response corresponds to the unexcited material when $\omega_p \to 0$ and is assumed to decrease linearly from that of the unexcited material n_0^2 with the degree of excitation according to

$$\epsilon_B = n_0^2 - \frac{n_0^2 - 1}{\rho_{tot}}\rho_{con}, \tag{2}$$

where ρ_{con} is the total density of conduction-band electrons and ρ_{tot} is the total number of valence-band electrons prior to excitation. The plasma frequency is defined as

$$\omega_p = \sqrt{\frac{e^2\rho_{con}}{\epsilon_0 m_e^*}}, \tag{3}$$

where e is the elementary charge, ϵ_0 is the vacuum permittivity, and m_e^* is the effective mass of conduction-band electrons.

The scattering rate Γ in Eq. (1) is, in general, a dynamic quantity which depends on the density of conduction-band electrons and their average energy above the conduction-band minimum $\langle\epsilon_{kin}\rangle$. Using a hard-sphere scattering model for carrier-carrier collisions and using the Debye screening radius as the radii of the scattering particles, a scattering rate can be derived [5,30]:

$$\Gamma_{c-c} = \frac{4\pi\epsilon_0}{e^2}\sqrt{\frac{6}{m_e^*}}\left(\frac{2}{3}\langle\epsilon_{kin}\rangle\right)^{3/2}. \tag{4}$$

Scattering between electrons and phonons also contribute to the overall scattering rate in the Drude model. Hence, the total scattering rate is taken to be the sum of two contributions $\Gamma = \Gamma_{e-ph} + \Gamma_{c-c}$ [5], where it is assumed that Γ_{e-ph} is constant.

Equation (1) shows how the optical properties of the dielectric will change drastically as electrons are excited to the conduction band, typically resulting in an increased absorption and surface reflectivity. The changes in ϵ, and thereby $\tilde{n}$, thus affect the electric field amplitude of pulses propagating through the dielectric. For a harmonic electric field **E** propagating in a homogeneous material with refractive index $\tilde{n}$, the relation between the intensity and electric field inside the dielectric is [31]

$$I = \langle S \rangle = \frac{1}{2}\epsilon_0 cn|\mathbf{E}|^2, \tag{5}$$

where c is the speed of light and $\langle S \rangle$ is the cycle-averaged Poynting vector.

B. The multiple rate equations model

The MRE model describes the dielectric using a single valence band and a conduction band divided into energetically equidistant levels, separated by the laser photon energy [14]. The strong-field excitation of the dielectric by a short laser pulse is described using Keldysh theory [8] and is considered only from the valence-band level to the lowest conduction-band level. The conduction-band electrons are excited to the next higher level due to absorption of the plasma. In our implementation of the MRE model, the rate of plasma absorption is calculated based on the imaginary part of the refractive index κ [5,32]. Once electrons have gained a sufficient amount of kinetic energy, they can contribute to collisional excitation, in which they collide with valence-band electrons and both the energetic electron and the valence-band electron end up in the conduction band. In our model, a constant rate of collisional excitation is assigned to all electrons capable of driving this process. Mathematically, this is all summarized in a set of N coupled differential equations, where N is the number of conduction-band levels included. They can be written as [2,5]

$$\frac{\partial\rho_1}{\partial t} = \dot{\rho}_{SFI}(|\mathbf{E}|)\frac{\rho_{val}}{\rho_{tot}} - W_{pl}\rho_1$$

$$+ \alpha\frac{\rho_{val}}{\rho_{tot}}\sum_{i'=2}^{N}\{\rho_{i'}\Theta[\epsilon_{kin}(i') - \epsilon_{coll}(|\mathbf{E}|)]\Upsilon(\Delta\tilde{\epsilon}(i'))\}$$

$$\vdots$$

$$\frac{\partial\rho_i}{\partial t} = W_{pl}(\rho_{i-1} - \rho_i) - \alpha\frac{\rho_{val}}{\rho_{tot}}\rho_i\Theta[\epsilon_{kin}(i) - \epsilon_{coll}(|\mathbf{E}|)]$$

$$+ \alpha\frac{\rho_{val}}{\rho_{tot}}\sum_{i'=i+1}^{N}\{\rho_{i'}\Theta[\epsilon_{kin}(i') - \epsilon_{coll}(|\mathbf{E}|)]$$

$$\times \Upsilon[\Delta\tilde{\epsilon}(i') - (i-1)]\}$$

$$\vdots$$

$$\frac{\partial\rho_N}{\partial t} = W_{pl}\rho_{N-1} - \alpha\frac{\rho_{val}}{\rho_{tot}}\rho_N\Theta[\epsilon_{kin}(N) - \epsilon_{coll}(|\mathbf{E}|)], \tag{6}$$

where **E** is the electric field, ρ_i is the electron density in the ith level, $\dot{\rho}_{SFI}$ is the strong-field excitation rate calculated from Keldysh theory [2,8], ρ_{val} is the number of remaining valence-band electrons, and W_{pl} is the plasma absorption rate [5,33],

$$W_{pl} = \frac{2\kappa\omega}{c}\frac{I}{\hbar\omega}\frac{1}{\rho_{con}} = \frac{\Gamma}{2\hbar\omega}\frac{e^2|\mathbf{E}|^2}{m_e^*(\omega^2 + \Gamma^2)}, \tag{7}$$

where $\rho_{con} = \sum_{i=1}^{N}\rho_i$ and the second equality follows from Eqs. (1) and (5). Furthermore, α is the constant collisional-excitation rate, Θ is the Heaviside step function, $\epsilon_{kin}(i)$ is the energy of the ith level with respect to the conduction-band minimum, and ϵ_{coll} is the energy needed to perform collisional

excitation while satisfying energy and momentum conservation [18],

$$\epsilon_{\text{coll}} = \frac{1 + 2\mu}{1 + \mu}\tilde{\epsilon}_G, \tag{8}$$

with $\tilde{\epsilon}_G$ being the effective band gap, which is the sum of the band gap ϵ_G prior to excitation and the ponderomotive energy $U_p = \frac{e^2|\mathbf{E}|^2}{4m_e^*\omega^2}$ [8]. $\mu = m_e^*/m_h^*$ is the ratio of the effective electron and hole mass. In the simulations presented in this paper, calculations are carried out with $\mu = 1$, which was also the case in previous works [5,19,20]. For further elaboration on this choice, see the discussion in Sec. IV.

The function Υ in Eq. (6) determines which levels are populated by electrons that have undergone collisional excitation to ensure energy conservation, and it is defined as [5]

$$\Upsilon(x) = \begin{cases} 2 & \text{if} \quad 0 \leqslant |x| \leqslant 0.25, \\ 1 & \text{if} \quad 0.25 < |x| < 0.75, \\ 0 & \text{otherwise.} \end{cases} \tag{9}$$

This function takes $\Delta\tilde{\epsilon}$ as an argument, which is a dimensionless quantity,

$$\Delta\tilde{\epsilon}(i) = \frac{1}{3}\left(i - 1 - \frac{\tilde{\epsilon}_G(|\mathbf{E}|)}{\hbar\omega}\right). \tag{10}$$

An important property of the MRE model is that it makes no assumption of a thermalized energy distribution of the conduction-band electrons and hence is able to describe out-of-equilibrium dynamics. On the other hand, in its form in Eq. (6), thermalization is not included, and hence, the model should, in principle, not be used to describe excitation with longer pulses where thermalization may have an effect, and we will in this work show only results using pulse durations up to 120 fs.

The MRE model was previously proven to be capable of describing both time-resolved reflectivity and phase-shift measurements, as well as fluence thresholds and hole depths [19,20].

C. Methods of propagation

1. Intensity propagation

To propagate the laser pulse in terms of its intensity envelope, the material is discretized into slabs along the propagation direction. The incoming intensity profile is determined from the peak fluence F_0 and the full width at half maximum pulse duration τ as

$$I(t) = \sqrt{\frac{4\ln(2)}{\pi}}\frac{F_0}{\tau}\exp\left[-4\ln(2)\left(\frac{t}{\tau}\right)^2\right]. \tag{11}$$

For each slab, the degree of excitation is solved as a function of time. Reflection from the first layer is accounted for by applying the Fresnel equations at normal incidence [34],

$$R(t) = \left|\frac{1 - \tilde{n}}{1 + \tilde{n}}\right|^2. \tag{12}$$

As the pulse propagates through a slab of material, the degree of excitation is calculated, thus giving the optical properties of the material as a function of time. These are then used to
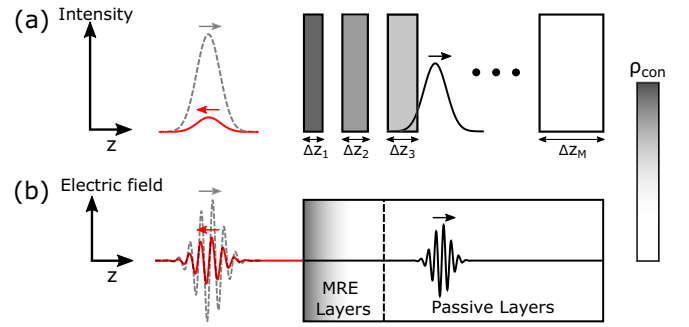

FIG. 1. Illustrations of the working principle of the two methods of propagation. (a) Intensity propagation: The material is divided into M slabs of exponentially increasing thickness Δz_m. The pulse is propagated through each slab individually by first obtaining the degree of excitation for each point in time along the pulse and then calculating the reduction in intensity for each of these points according to Eq. (13). (b) FDTD propagation: The entire calculation region is divided into slabs of constant thickness Δz. The MRE model is solved for the first part of the material, while the remaining material remains unexcited. In both (a) and (b) the arrows mark the direction of propagation, and the dashed gray lines represent the incoming pulses.

propagate the pulse to the adjacent layer by using [5]

$$\frac{\partial I}{\partial z} = -\left(\frac{2\kappa\omega}{c} + \frac{\rho_{\text{val}}}{\rho_{\text{tot}}}\left\lceil\frac{\tilde{\epsilon}_G}{\hbar\omega}\right\rceil\hbar\omega\dot{\rho}_{\text{SFI}}\frac{1}{I}\right)I = -\beta I, \tag{13}$$

where $\lceil\cdot\rceil$ is the ceil operator. The first term in Eq. (13) accounts for the Drude absorption in the material, and the second term accounts for the energy lost from the laser field due to strong-field excitation. In practice, each temporal component of the pulse is propagated to the next layer according to

$$I(t, z_{m+1}) = I(t, z_m)[1 - \beta(t, z_m)\Delta z_m], \tag{14}$$

where m is a spatial index for the different layers. Figure 1(a) illustrates the working principle of the intensity propagation technique. In the calculations presented in this paper, the intensity propagation was carried out by dividing a 300 nm bulk sample into 100 slabs of exponentially increasing thickness to reduce computational time.

2. Finite-difference time-domain method

In the model presented in the current paper, Maxwell's equations are solved using the finite-difference time-domain (FDTD) method [35,36] in one dimension by considering an electric field linearly polarized in the x direction propagating along the z direction. Formulated in the frequency domain, the relevant Maxwell's equations are [34]

$$\nabla \times \mathbf{E}(\omega) = -i\omega\mu_0\mathbf{H}(\omega), \tag{15}$$

$$\nabla \times \mathbf{H}(\omega) = i\omega\epsilon_0\epsilon_B\mathbf{E}(\omega) + \mathbf{J}_{\text{Drude}}(\omega) + \mathbf{J}_{\text{SFI}}(\omega). \tag{16}$$

Here, the dielectric function from Eq. (1) has been inserted into Ampere's law [Eq. (16)], and an additional current density term $\mathbf{J}_{\text{SFI}}$ has been added. The first term in Eq. (16) corresponds to the current density in a nondispersive dielectric with refractive index $\sqrt{\epsilon_B}$. The second term is interpreted as

a polarization current density generated by the free carriers described by the Drude model and is given by

$$\mathbf{J}_{\text{Drude}}(\omega) = -i\omega\epsilon_0 \frac{\omega_p^2}{\omega^2 + i\Gamma\omega}\mathbf{E}(\omega). \qquad (17)$$

The last term, $\mathbf{J}_{\text{SFI}}$, is a fictive current density induced by strong-field excitation, which ensures energy conservation. In the time domain it is given by [26,37,38]

$$\mathbf{J}_{\text{SFI}}(t) = \frac{\rho_{\text{val}}}{\rho_{\text{tot}}}\frac{\dot{\rho}_{\text{SFI}}\tilde{\epsilon}_G}{|\mathbf{E}(t)|^2}\mathbf{E}(t). \qquad (18)$$

It should be understood that all material parameters are spatially dependent and correspond to vacuum parameters outside the material.

To solve for $\mathbf{E}$ and $\mathbf{H}$ in the time domain, we make use of the *auxiliary differential equation* method [39,40]. Here, Eq. (17) is Fourier transformed, and a differential equation is obtained for $\mathbf{J}_{\text{Drude}}(t)$. The Drude current density is solved for in every time step and is inserted back into Maxwell's equations in the time domain along with $\mathbf{J}_{\text{SFI}}(t)$ to obtain solutions for $\mathbf{E}(t)$ and $\mathbf{H}(t)$. The incoming *complex* electric field is generated as a hard source at one of the simulation boundaries as

$$\mathbf{E} = E_0 e^{-i\omega t}\exp\left[-2\ln(2)\left(\frac{t}{\tau}\right)^2\right]\hat{\mathbf{x}}, \qquad (19)$$

where E_0 is the maximum electric field amplitude. It should be noted that the actual field is $\text{Re}(\mathbf{E})$. When evaluating the strong-field excitation rate, the absolute value $|\mathbf{E}|$ is used, which is consistent with Keldysh theory [8] and with the intensity propagation method of using Eqs. (5) and (11). The material parameters are updated in every time step according to the value of the electric field.

For the results presented here, Eqs. (15) and (16) are solved with a spatial resolution of $\Delta z = 10$ nm and with a time step of $\Delta t = \Delta z/c \approx 33.4$ as, which is known as the Courant-Friedrichs-Lewy condition [36]. The MRE model is solved for only the first 5 μm into the sample, while the remaining material retains the properties of the unexcited material. This depth is chosen such that for fluences close to and above the ablation threshold, the mismatch in the refractive index between the last excited spatial layer and the next unexcited passive layer is small enough to give no significant reflection that would otherwise affect the output of the simulation. At lower fluences, where penetration of the excitation is deeper, one should increase the depth at which the MRE model is solved. Figure 1(b) illustrates the working principle of the FDTD propagation method.

III. RESULTS

A. Excitation dynamics

The results of the combined MRE and FDTD model are illustrated in Fig. 2. The calculation provides the electric field as well as the carrier distribution as a function of time for all simulated depths. The model parameters correspond to sapphire (see Table I). Most of the model parameters are taken from the literature while two parameters are tuned in order to obtain the best agreement with the crater profiles from
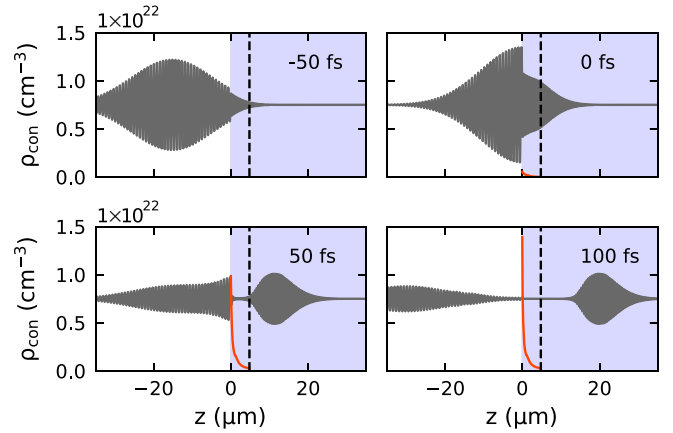

FIG. 2. Snapshots of the material-excitation and light-propagation dynamics. The laser pulse has a pulse duration of 58 fs, a peak fluence of 4.5 J cm^{-2}, and a central wavelength of 800 nm. Note that the snapshots show a zoom of the computational window. The four panels show the electric field (scale not shown) and the conduction-band-electron density versus depth (red line) for four different time delays (with $t = 0$ fs corresponding to the time when the peak of the electric field strikes the surface). A full animation of the dynamics is available in the Supplemental Material [41].

Ref. [46]: the density of conduction-band electrons needed to cause ablation ρ_{ablation} and the collisional-excitation rate α.

Figure 2 illustrates how the model nicely captures the expected excitation dynamics. The front end of the pulse (at $t = -50$ fs) sees a dielectric material. It undergoes normal Fresnel reflection at the surface but propagates mostly undisturbed into the material. As the electric field increases at later times, the carrier concentration increases (red curve), and this has a pronounced influence on the electric field propagation, with a large fraction of the light being absorbed by the plasma. Note that Fig. 2 represents frames from an animation showing the detailed time evolution of excitation and propagation. The animation is available in the Supplemental Material [41].

B. Prediction of key ablation parameters

From the two material-excitation models, we are able to simulate key observables measured in laser-ablation experiments reported in the literature. We choose the ablation criterion and the collisional-excitation rate so that the model

TABLE I. Parameters used for the MRE to describe sapphire.

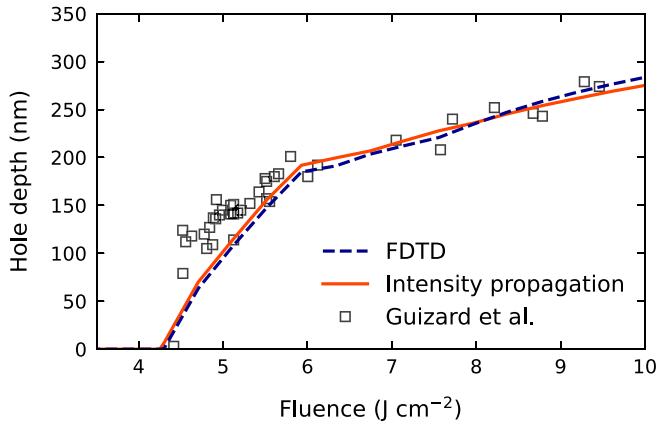| Parameter	Value	References
n_0	1.76	[42]
ϵ_G	9.9 eV	[43,44]
m_e^*	$0.38 m_e$	[44,45]
m_h^*	$3.99 m_e$	[44,45]
ρ_{tot}	2.8×10^{23} cm^{-3}	[44]
ρ_{ablation}	4% of ρ_{tot}	
α	0.5×10^{15} s^{-1}	
$\Gamma_{\text{e-ph}}$	1×10^{14} s^{-1}	
N	100	

FIG. 3. Calculated hole depth in sapphire as a function of laser fluence using the FDTD propagation and the intensity propagation for a 58 fs pulse with a central wavelength of 800 nm. The model parameters used are from Table I. A comparison is shown with experimental data from Guizard *et al.* [46].
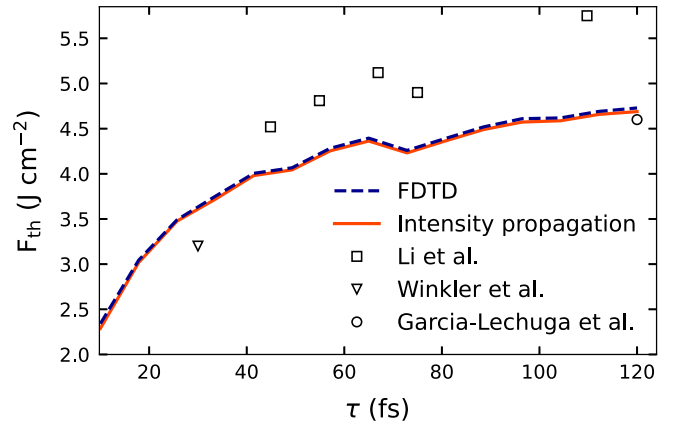

FIG. 4. The ablation threshold versus pulse duration for sapphire calculated using FDTD propagation and intensity propagation for pulses with a central wavelength of 800 nm. The model parameters used are from Table I. A comparison is shown with experimental data from Li *et al.* [48], Winkler *et al.* [47], and Garcia-Lechuga *et al.* [44].

agrees with experimental data for crater profiles from Guizard *et al.* [46]. First, we explore the predicted hole depths for the two models for a central laser wavelength of 800 nm and a pulse duration of $\tau = 58$ fs for a range of fluences, and we then determine how the ablation threshold scales with the pulse duration in the surface layer.

1. Hole depth versus fluence

To determine the depths of holes predicted by the two models, the depth at which $\rho = \rho_{ablation}$ is calculated for a series of laser fluences. In the case of the FDTD simulations, it is ensured that the pulse has fully propagated through the region of high excitation and that the carrier dynamics has reached a steady state.

Figure 3 shows good agreement between the two methods of propagation, which indicates that using a Lambert-Beer approach [Eq. (13)] for the pulse propagation is valid in the case of bulk dielectrics, which could not *a priori* be expected, as discussed in detail later. We also see that both models show good agreement with the experimental data from Ref. [46] after adjusting only two parameters to that data set.

2. Threshold fluence versus pulse duration

To determine the ablation threshold for each of the two propagation models, we determine the fluence at which $\rho_{con} = \rho_{ablation}$. In the case of the intensity propagation, only a single layer is included, whereas in the FDTD propagation, the simulation is stopped when the carrier dynamics at the surface reaches a steady state. In practice, finding F_{th} for a specific $\rho_{ablation}$ is an optimization problem, which is solved with an accuracy of 0.01 J/cm^2.

Figure 4 again shows excellent agreement between the two methods of propagation, thus showing that the intensity propagation method is adequate when considering bulk ablation. The simulated results are compared to experimental data from several sources, all using 800 nm Ti:sapphire lasers in single-shot operation. The general pulse-duration dependence of the ablation threshold seems to be captured by the model.

The data from Li *et al.* suggest that our model underestimates the ablation threshold, especially at longer pulse durations, while the individual data points from Winkler *et al.* [47] and Garcia-Lechuga *et al.* [44] show better agreement. We note that ablation thresholds reported in the literature vary significantly for all dielectrics and only a small number of studies on single-shot ablation of sapphire exist.

C. Excitation of a freestanding thin film

An advantage of formulating the laser pulse in terms of its electric field is that interference within the dielectric is automatically accounted for. Interference is particularly important when ablating thin films whenever there is a significant refractive-index mismatch between the film and its substrate [49]. This was demonstrated experimentally in the excitation of 1 μm SiO$_x$ films on silicon substrates [29], where it was shown that due to the formation of periodic plasma disks [28,29] in the depth of the film, the removal of film was divided into several layers for high fluences. The same phenomenon is predicted by our model, and we show it here in the case of a freestanding dielectric film with a thickness of 910 nm with material properties corresponding to sapphire excited by a 58 fs 800 nm laser pulse in Fig. 5. The thickness was chosen to be $\sim 4 \times \lambda/(2n_0)$ such that an interference maximum is present on the front surface and we see several interference maxima. Figure 5 illustrates the importance of incorporating interference into the excitation in the case of thin films. The interference between the incoming and reflected waves leads to periodic regions of alternating high and low excitation. It may be noted that although the reflectivity of the sapphire-air interface is only 7.6%, interference has a large impact on the degree of excitation due to the nonlinear excitation mechanism. It also becomes apparent that interference within the film significantly affects the ablation threshold. In particular, one might expect a near-stepwise increase in hole depth, corresponding to separated ejected layers, as a function of fluence, as indicated by the blue and red solid lines in Fig. 5 corresponding to the ejection of one and two
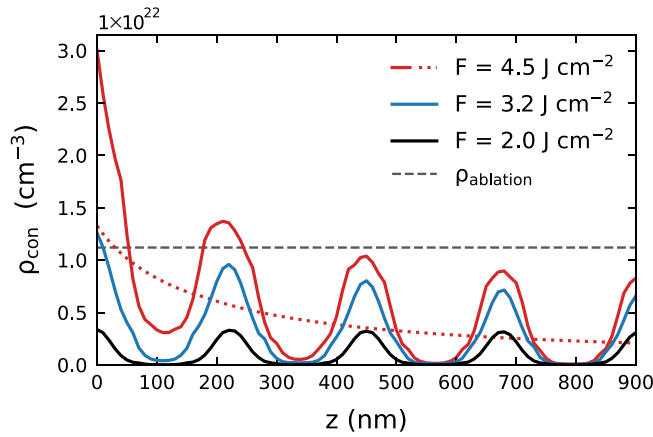
FIG. 5. A model prediction of the degree of excitation as a function of the depth for a freestanding 910 nm thick film of sapphire irradiated by a 58 fs pulse with a central wavelength of 800 nm for three different fluences (solid lines). For the highest fluence, a calculation is shown for a bulk sample by the red dotted line. The dashed gray line shows the ablation criterion. The model parameters used are from Table I.
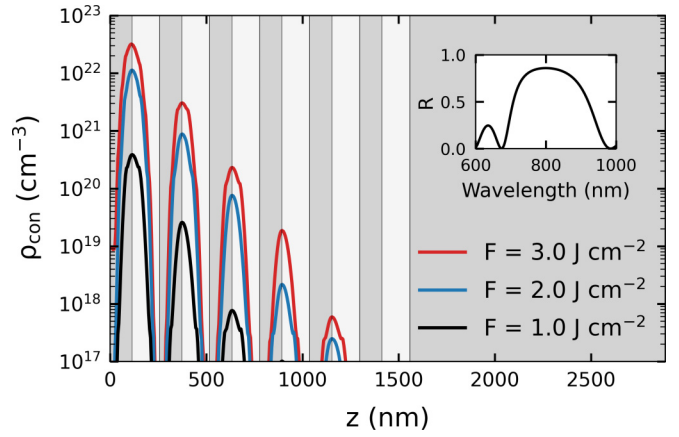

FIG. 6. Calculated excitation as a function of depth through an 800 nm mirror for a 58 fs pulse with a central wavelength of 800 nm. Darker layers correspond to sapphire, and lighter layers correspond to MgF_2. The model parameters used are from Table I, except for the refractive index of MgF_2, which is 1.375. The inset shows the reflectivity as a function of the wavelength of the dielectric coating calculated using the transfer-matrix method implementation from [52].

layers, respectively. We note that for this to be observed, the unexcited material must be ejected out of the surface, which depends entirely on the dynamics of the ablation and is not included in our model. However, even if the material is not ejected, the present model can still be used to determine the ablation threshold for such structures even if ablation is not visible at the surface. The reason why the fluence determines the number of ejected layers in our model is that for fluences far below the bulk ablation threshold, the propagation of the pulse is mostly unaffected by the excitation, leaving the excitation and propagation largely uncoupled. This leads to an excitation profile which mimics that of the intensity distribution inside of a Fabry-Pérot etalon. For fluences close to and above the bulk ablation threshold, excitation and propagation become coupled. This is caused by the pulse being able to effectively excite the material without the presence of constructive interference. Hence, as the pulse propagates towards the rear surface and back towards the front surface, it is already strongly absorbed, leading to a weaker effect of interference close to the front surface. The fact that thin film interference can heavily affect the threshold for laser ablation is clearly demonstrated by the solid and dotted red lines in Fig. 5, which compare the excitation versus depth for the freestanding thin film (solid) and bulk sample (dotted) for the same laser fluence. The electron density in the conduction band at the surface of the freestanding thin film is more than twice as high as that of the bulk sample. Note that whenever the substrate, in this case air, has a lower refractive index than the film, the rear surface will always be an interference maximum because the phase of the reflected light is preserved [34]. On the other hand, depending on the film thickness, the constructive interference closest to the front surface may shift significantly away from the surface such that one may already be ablating the bulk before observing surface ablation. Last, it should be noted that interference within a thin film as shown here occurs only if the longitudinal spatial extent of the pulse

within the film (i.e., $c\tau/n_0$) is significantly larger than the film thickness.

D. Excitation of a dielectric mirror

A very relevant application of the model is to calculate the excitation of dielectric coatings such as high-reflectivity or antireflective coatings. From the properties of each material used in the stack of dielectric thin films, one can directly determine ablation thresholds for the dielectric stack. This could, for instance, be used to design more durable dielectric mirrors for intense-laser applications. To illustrate this, we simulate a dielectric stack corresponding to an 800 nm dielectric mirror of alternating layers of sapphire with model parameters according to Table I and MgF_2. For simplicity, we use the same material parameters for MgF_2 and change only the refractive index to $n_{MgF_2} = 1.375$ [50]. To produce a dielectric mirror, the layer thickness of each material must be $\lambda/(4n)$ [51], and the material with the highest refractive index must be located at the surface. Figure 6 shows the degree of excitation (on a logarithmic scale) as a function of depth through the dielectric mirror for different fluences. As expected, the highest excitation appears at depths of constructive interference, which in a dielectric mirror is at the interface when going from a high to low refractive index. This is again because reflected waves at these interfaces preserve the phase, and thus, these depths will always correspond to antinodes of the electric field, while interfaces going from a low to high refractive index will be nodes and thus will experience low excitation. It is observed that the high excitation is located primarily close to the front surface, which is expected since reflections cause the intensity to decrease as light penetrates further into the dielectric stack. Since the intensity is at a maximum exactly at the interface between the two materials, one must then expect the material that has the smaller ablation threshold to determine the overall ablation threshold for the coating. The same conclusion was

reached by Jasapara *et al.* [27] using an SRE model combined with a local intensity factor from linear propagation and was also demonstrated by Zhang *et al.* [24] using FDTD combined with a variation of the SRE model.

IV. DISCUSSION

The model presented here is an elaboration on previous implementations of the MRE model [5,14], and the results can both serve as a benchmark for the previous implementations and allow for calculations influenced by interference. A key difference between the two methods is that propagation of the intensity envelope using a Lambert-Beer approach (Eq. 13) assumes that reflections from the bulk are negligible. Since we are in a regime where the spatial changes of the dielectric function are substantial over the wavelength scale, this cannot *a priori* be expected. Our model based on a direct solution of Maxwell's equations shows that this must be a negligible effect, even though the critical density is reached inside the material. This suggests that the computationally less expensive intensity propagation method can be applied when simulating propagation through bulk samples. However, FDTD has the advantage that linear dispersion from the Drude plasma is directly accounted for in the propagation. While dispersion of the unexcited dielectric has been neglected here for simplicity, it could easily be incorporated simply by using a Drude-Lorentz optical model and adding the appropriate current density term in Eq. (15).

In this paper, Maxwell's equations have been solved only in the one-dimensional case, which has primarily been for simplicity and to reduce computational time. While a similar two-dimensional analysis could be done, the large number of coupled differential equations in the MRE model would make such calculations time-consuming. For such calculations it might be appealing to utilize a computationally less demanding laser-matter interaction model, such as the SRE model. Attempts were made to simulate ablation thresholds and hole depths with an SRE model, but we were unsuccessful in finding a set of physically meaningful parameters that could reproduce the experimental data. A better alternative seems to be the *dynamical rate equations* (DRE) model, proposed by Déziel *et al.* [33], which is a simplification of the MRE model, in which the assumption of a Maxwellian distribution of the excited carriers (which was also used in [22,24]) reduces the number of coupled differential equations to just two. It was shown that for a properly chosen set of material parameters, the DRE model could produce results similar to those of the MRE model using the original formulation from [14]. Two- or three-dimensional propagation opens up the ability to investigate effects of nonlinear field propagation [53] or more complex material geometries.

When determining the parameters for the MRE model, it was observed that for the known effective masses for sapphire, ϵ_{coll} became quite small, which gave rise to very efficient avalanche excitation, meaning that the model did not agree with experimental data. Rather than using the effective masses as a fitting parameter, as was done in other studies [33], we used the known effective masses of the band structure to calculate the strong-field ionization rate and ponderomotive energy, while the free electron mass was used to calculate ϵ_{coll}

for both electrons and holes. Our reasoning behind this is that the strong-field excitation process occurs primarily from the valence-band maximum to the conduction-band minimum and hence is a process for which the approximation of parabolic bands is mostly valid. For the case of collisional excitation, however, the electrons capable of driving this process reside far from the band edge where the parabolic approximation is undoubtedly very poor. Instead, they are expected to behave more like free electrons, and hence, a value of $\mu = 1$ has been used. The consequence of this is that it always takes an energy $\frac{3}{2}\epsilon_G$ above the conduction-band minimum for collisional excitation to be allowed, as opposed to $1.09\epsilon_G$ that would otherwise be the case for sapphire.

Several time-resolved experiments have shown delayed onset of reflectivity of probe pulses with respect to the exciting pump [7,54,55]. This phenomenon seems not to be explained through the MRE model in its current form. Reference [7] suggested that the effect is due to band filling and Pauli blocking. In general, it could be speculated that energetic electrons behave optically differently from those close to the conduction-band edge, in part because the effective mass changes and in part because the scattering rate is significantly different. In that case, the delayed onset of reflectivity could be a sign of thermalization of the conduction-band electrons. This can be incorporated into the MRE model but would add an additional layer of complexity as well as additional free parameters.

Carrier diffusion has not been considered in this paper, which is common when simulating carrier dynamics in dielectrics [5,24,33]. The reason is that the low carrier mobilities in dielectrics makes the timescale for carrier transport significantly longer than the timescale for excitation and local carrier dynamics. It has, however, been proposed that due to the high temperatures and the marked difference in mobilities between electrons and holes, large electric fields may be generated as carrier separation occurs [56]. It was proposed that this could be linked to an observed strong difference in the *s* and *p* reflectivities of fused silica in a time-resolved reflectivity measurement [7]. To include such effects it would be necessary to incorporate diffusion into our model. Although its effects on ablation are unclear, it would have measurable effects on reflectivity and transmission and result in a predicted emission of terahertz radiation [56]. In particular, it could be interesting to investigate how carrier diffusion may play a role in the optical response of excited thin films because the strong gradients in the conduction-band electron density (Fig. 5) should enhance diffusion effects.

V. CONCLUSION

We have presented a model for simulating excitation of dielectrics in which the laser-matter interaction is described by the multiple rate equations model and the propagation of the laser pulse is carried out by solving Maxwell's equations using a Drude model for the optical response. Simulations of ablation thresholds and hole depths of sapphire were compared to a previously used method of propagation, yielding almost identical results, and both models show good agreement with existing experimental results. The advantages of our method of propagation were demonstrated by illustrating how

interference between incoming and reflected waves affects the level of excitation in a single freestanding thin film as well as a stack of dielectric films corresponding to a dielectric mirror at normal incidence for 800 nm.

[1] S. Mao, F. Quéré, S. Guizard, X. Mao, R. Russo, G. Petite, and P. Martin, Dynamics of femtosecond laser interactions with dielectrics, Appl. Phys. A **79**, 1695 (2004).

[2] P. Balling and J. Schou, Femtosecond-laser ablation dynamics of dielectrics: Basics and applications for thin films, Rep. Prog. Phys. **76**, 036502 (2013).

[3] B. C. Stuart, M. D. Feit, A. M. Rubenchik, B. W. Shore, and M. D. Perry, Laser-Induced Damage in Dielectrics with Nanosecond to Subpicosecond Pulses, Phys. Rev. Lett. **74**, 2248 (1995).

[4] W. Kautek, J. Krüger, M. Lenzner, S. Sartania, C. Spielmann, and F. Krausz, Laser ablation of dielectrics with pulse durations between 20 fs and 3 ps, Appl. Phys. Lett. **69**, 3146 (1996).

[5] B. H. Christensen and P. Balling, Modeling ultrashort-pulse laser ablation of dielectric materials, Phys. Rev. B **79**, 155424 (2009).

[6] I. Mirza, N. M. Bulgakova, J. Tomáštík, V. Michálek, O. Haderka, L. Fekete, and T. Mocek, Ultrashort pulse laser ablation of dielectrics: Thresholds, mechanisms, role of breakdown, Sci. Rep. **6**, 39133 (2016).

[7] S. H. Møller, S. T. Andersen, and P. Balling, Transient optical properties of highly excited dielectric materials: Apparent bire-fringence and delayed reflectivity increase, Phys. Rev. Res. **2**, 043010 (2020).

[8] L. V. Keldysh, Ionization in the field of a strong electromagnetic wave, Sov. Phys. JETP **20**, 1307 (1965).

[9] V. E. Gruzdev, Laser-induced ionization of solids: Back to Keldysh, in *Laser-Induced Damage in Optical Materials 2004*, International Society for Optics and Photonics, edited by G. J. Exarhos, A. H. Guenther, N. Kaiser, K. L. Lewis, M. J. Soileau, and C. J. Stolz (SPIE, 2005), Vol. 5647, pp. 480–492.

[10] N. Bloembergen, Laser-induced electric breakdown in solids, IEEE J. Quantum Electron. **10**, 375 (1974).

[11] B. C. Stuart, M. D. Feit, S. Herman, A. M. Rubenchik, B. W. Shore, and M. D. Perry, Optical ablation by high-power short-pulse lasers, J. Opt. Soc. Am. B **13**, 459 (1996).

[12] M. Lenzner, J. Krüger, S. Sartania, Z. Cheng, C. Spielmann, G. Mourou, W. Kautek, and F. Krausz, Femtosecond Optical Breakdown in Dielectrics, Phys. Rev. Lett. **80**, 4076 (1998).

[13] M. Mero, J. Liu, W. Rudolph, D. Ristau, and K. Starke, Scaling laws of femtosecond laser pulse induced breakdown in oxide films, Phys. Rev. B **71**, 115109 (2005).

[14] B. Rethfeld, Unified Model for the Free-Electron Avalanche in Laser-Irradiated Dielectrics, Phys. Rev. Lett. **92**, 187401 (2004).

[15] F. Quéré, S. Guizard, and P. Martin, Time-resolved study of laser-induced breakdown in dielectrics, Europhys. Lett. **56**, 138 (2001).

[16] P. P. Rajeev, M. Gertsvolf, P. B. Corkum, and D. M. Rayner, Field Dependent Avalanche Ionization Rates in Dielectrics, Phys. Rev. Lett. **102**, 083001 (2009).

[17] D. Grojo, M. Gertsvolf, S. Lei, T. Barillot, D. M. Rayner, and P. B. Corkum, Exciton-seeded multiphoton ionization in bulk SiO$_2$, Phys. Rev. B **81**, 212301 (2010).

[18] A. Kaiser, B. Rethfeld, M. Vicanek, and G. Simon, Microscopic processes in dielectrics under irradiation by subpicosecond laser pulses, Phys. Rev. B **61**, 11437 (2000).

[19] K. J. Wædegaard, D. B. Sandkamm, A. Mouskeftaras, S. Guizard, and P. Balling, Probing ultrashort-pulse laser excitation of sapphire: From the initial carrier creation to material ablation, Europhys. Lett. **105**, 47001 (2014).

[20] L. Haahr-Lillevang, K. Wædegaard, D. Sandkamm, A. Mouskeftaras, S. Guizard, and P. Balling, Short-pulse laser excitation of quartz: experiments and modelling of transient optical properties and ablation, Appl. Phys. A **120**, 1221 (2015).

[21] P. Balling, Laser coupling and relaxation of the absorbed energy: Metals, semiconductors, and dielectrics, in *Handbook of Laser Micro- and Nano-engineering*, edited by K. Sugioka (Springer, Cham, 2020), pp. 1–58.

[22] J. R. Peñano, P. Sprangle, B. Hafizi, W. Manheimer, and A. Zigler, Transmission of intense femtosecond laser pulses into dielectrics, Phys. Rev. E **72**, 036412 (2005).

[23] G. Duchateau and A. Bourgeade, Influence of the time-dependent pulse spectrum on ionization and laser propagation in nonlinear optical materials, Phys. Rev. A **89**, 053837 (2014).

[24] S. Zhang, C. Menoni, V. Gruzdev, and E. Chowdhury, Ultrafast laser material damage simulation—A new look at an old problem, Nanomaterials **12**, 1259 (2022).

[25] R. Beuton, B. Chimier, P. Quinoman, P. González Alaiza de Martínez, R. Nuter, and G. Duchateau, Numerical studies of dielectric material modifications by a femtosecond Bessel–Gauss laser beam, Appl. Phys. A **127**, 334 (2021).

[26] B. Morel, R. Giust, K. Ardaneh, and F. Courvoisier, Two-fluid plasma model for ultrashort laser-induced electron-hole nanoplasmas, Phys. Rev. B **106**, 035207 (2022).

[27] J. Jasapara, A. V. V. Nampoothiri, W. Rudolph, D. Ristau, and K. Starke, Femtosecond laser pulse induced breakdown in dielectric thin films, Phys. Rev. B **63**, 045117 (2001).

[28] K. Kumar, K. K. Lee, J. Li, J. Nogami, N. P. Kherani, and P. R. Herman, Quantized structuring of transparent films with femtosecond laser interference, Light: Sci. Appl. **3**, e157 (2014).

[29] D. M. Roper, S. Ho, M. Haque, P. Jha, and P. R. Herman, Inhibition and enhancement of quantized, interference-driven, ultrafast-laser cleaving, and intrafilm ejection with angle and polarization control, Adv. Mater. Technol. **3**, 1700234 (2018).

[30] A. Rämer, L. Haahr-Lillevang, B. Rethfeld, and P. Balling, Modeling the transient optical parameters in laser-excited band gap materials, Opt. Eng. **56**, 011015 (2016).

[31] R. Loudon, The propagation of electromagnetic energy through an absorbing dielectric, J. Phys. A **3**, 233 (1970).

[32] K. Wædegaard, D. Sandkamm, L. Haahr-Lillevang, K. Bay, and P. Balling, Modeling short-pulse laser excitation of dielectric materials, Appl. Phys. A **117**, 7 (2014).

[33] J.-L. Déziel, L. J. Dubé, and C. Varin, Dynamical rate equation model for femtosecond laser-induced breakdown in dielectrics, Phys. Rev. B **104**, 045201 (2021).

[34] J. D. Jackson, *Classical Electrodynamics*, 3rd ed. (Wiley, New York, 1999).

[35] K. Yee, Numerical solution of initial boundary value problems involving Maxwell's equations in isotropic media, IEEE Trans. Antennas Propag. **14**, 302 (1966).

[36] U. S. Inan and R. A. Marshall, *Numerical Electromagnetics: The FDTD Method* (Cambridge University Press, Cambridge, 2011).

[37] S. C. Rae and K. Burnett, Detailed simulations of plasma-induced spectral blueshifting, Phys. Rev. A **46**, 1084 (1992).

[38] P. Mulser, F. Cornolti, and D. Bauer, Modeling field ionization in an energy conserving form and resulting nonstandard fluid dynamics, Phys. Plasmas **5**, 4466 (1998).

[39] T. Kashiwa and I. Fukai, A treatment by the FD-TD method of the dispersive characteristics associated with electronic polarization, Microwave Opt. Technol. Lett. **3**, 203 (1990).

[40] R. M. Joseph, S. C. Hagness, and A. Taflove, Direct time integration of Maxwell's equations in linear dispersive media with absorption for scattering and propagation of femtosecond electromagnetic pulses, Opt. Lett. **16**, 1412 (1991).

[41] See Supplemental Material at http://link.aps.org/supplemental/10.1103/PhysRevB.108.094307 for a full animation of the excitation dynamics.

[42] M. N. Polyanskiy, Refractive index database, https://refractiveindex.info.

[43] E. Arakawa and M. Williams, Optical properties of aluminum oxide in the vacuum ultraviolet, J. Phys. Chem. Solids **29**, 735 (1968).

[44] M. Garcia-Lechuga, L. Haahr-Lillevang, J. Siegel, P. Balling, S. Guizard, and J. Solis, Simultaneous time-space resolved reflectivity and interferometric measurements of dielectrics excited with femtosecond laser pulses, Phys. Rev. B **95**, 214114 (2017).

[45] J. E. Medvedeva, E. N. Teasley, and M. D. Hoffman, Electronic band structure and carrier effective mass in calcium aluminates, Phys. Rev. B **76**, 155107 (2007).

[46] S. Guizard, A. Semerok, J. Gaudin, M. Hashida, P. Martin, and F. Quéré, Femtosecond laser ablation of transparent dielectrics: Measurement and modelisation of crater profiles, Appl. Surf. Sci. **186**, 364 (2002).

[47] T. Winkler, L. Haahr-Lillevang, C. Sarpe, B. Zielinski, N. Götte, A. Senftleben, P. Balling, and T. Baumert, Laser amplification in excited dielectrics, Nat. Phys. **14**, 74 (2018).

[48] X. Li, T. Jia, D. Feng, and Z. Xu, Ablation induced by femtosecond laser in sapphire, Appl. Surf. Sci. **225**, 339 (2004).

[49] J. Bonse and J. Krüger, Structuring of thin films by ultrashort laser pulses, Appl. Phys. A **129**, 14 (2023).

[50] M. J. Dodge, Refractive properties of magnesium fluoride, Appl. Opt. **23**, 1980 (1984).

[51] M. Born, E. Wolf, A. B. Bhatia, P. C. Clemmow, D. Gabor, A. R. Stokes, A. M. Taylor, P. A. Wayman, and W. L. Wilcock, *Principles of Optics: Electromagnetic Theory of Propagation, Interference and Diffraction of Light*, 7th ed. (Cambridge University Press, Cambridge, 1999).

[52] E. H. Eriksen, tmmpy (0.0.9), Zenodo, 2018, https://doi.org/10.5281/zenodo.1344878.

[53] M. Fujii, M. Tahara, I. Sakagami, W. Freude, and P. Russer, High-order FDTD and auxiliary differential equation formulation of optical pulse propagation in 2-D Kerr and Raman nonlinear dispersive media, IEEE J. Quantum Electron. **40**, 175 (2004).

[54] D. Puerto, W. Gawelda, J. Siegel, J. Bonse, G. Bachelier, and J. Solis, Transient reflectivity and transmission changes during plasma formation and ablation in fused silica induced by femtosecond laser pulses, Appl. Phys. A **92**, 803 (2008).

[55] M. Garcia-Lechuga, J. Siegel, J. Hernandez-Rueda, and J. Solis, Imaging the ultrafast Kerr effect, free carrier generation, relaxation and ablation dynamics of lithium niobate irradiated with femtosecond laser pulses, J. Appl. Phys. **116**, 113502 (2014).

[56] S. H. Møller, P. S. Sneftrup, B. Julsgaard, and P. Balling, Carrier transport after ultrashort-pulse-laser excitation in dielectric materials leads to 10 MV/m electric fields: Transient birefringence and emission of THz radiation (unpublished).

Correction: A conversion error introduced during the production process in a value given in the seventh row of the second column of Table I has been fixed.